Core Excitation, Specific Dissociation, and the Effect of the Size of Aromatic Molecules Connected to Oxygen: Phenyl Ether and 1,3-Diphenoxybenzene

Yi-Shiue Lin,[†] Shu-Yu Lin,[†,‡] Yuan T. Lee,[‡] Chien-Ming Tseng,[§] Chi-Kung Ni,[‡,∥] Chen-Lin Liu,*,[†] Cheng-Cheng Tsai,[⊥] Jien-Lian Chen,[⊥] and Wei-Ping Hu*,[⊥]

[†]Scientific Research Division, National Synchrotron Radiation Research Center, Hsinchu 30076, Taiwan

[‡]Institute of Atomic and Molecular Sciences, Academia Sinica, P.O. Box 23-166, Taipei 10617, Taiwan

[§]Department of Applied Chemistry, National Chiao Tung University, Hsinchu 30010, Taiwan

[∥]Department of Chemistry, National Tsing Hua University, Hsinchu 30013, Taiwan

[⊥]Department of Chemistry and Biochemistry, National Chung Cheng University, Chia-Yi 62102, Taiwan

Ⓢ Supporting Information

ABSTRACT: Near-edge X-ray absorption fine structure (NEXAFS) spectra of phenyl ether at the carbon K-edge and 1,3-diphenoxybenzene at both the carbon and oxygen K-edges were measured in the total ion yield mode using X-rays from a synchrotron and a reflectron time-of-flight mass spectrometer. Time-dependent density functional theory was adopted to calculate the carbon and oxygen K-edge NEXAFS spectra of phenol, phenyl ether, and 1,3-diphenoxybenzene. The assignments and a comparison of the experimental and calculated spectra are presented. The mass spectra of ionic products formed after X-ray absorption at various excitation energies are also reported. Specific dissociations were observed for the $1s \rightarrow \pi^*$ transition of phenyl ether. In comparison with phenol and phenyl ether, the dependence of the fragmentation on the excitation site and destination state was weak in 1,3-diphenoxybenzene, likely as a result of delocalization of the valence electrons and rapid randomization of energy.
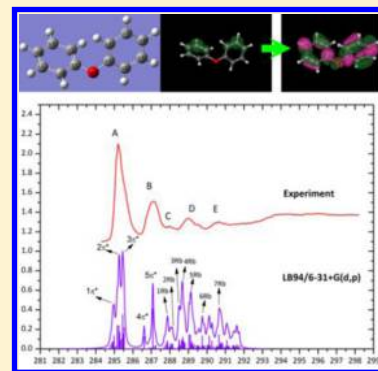
■ INTRODUCTION

In the early 1920s, the wavelengths of the X-ray absorption edge were discovered to depend on the chemical environment of atoms of a given element.[1,2] Near-edge X-ray absorption fine structure (NEXAFS) spectra have proved to be sensitive to the electronic structure of materials and useful for chemical analysis.[3−8] The shifts of soft X-ray absorption spectra for a given element due to varied chemical environments range from ∼0.2 eV to several eV. For example, the C 1s → $\pi^*_{C=O}$ excitation for a carbonate is blue-shifted by ∼4 eV relative to that for an aldehyde.[9] Similarly, the absorption energies of the carbon atom adjacent to the nitrogen atom in aniline and the carbon atom adjacent to the oxygen atom in phenol are blue-shifted by about 1.5 and 1.7 eV, respectively, relative to those of other carbon atoms in aniline, phenol, and benzene.[10]

When a molecule absorbs an X-ray photon, one core electron of a particular atom is excited to an empty valence orbital or is directly ionized, forming a hole in the inner shell of the atom. Auger decay is a major channel following excitation of a core electron. After emission of one or two electrons following Auger decay, the resulting molecular ions are generally unstable and dissociate into charged and neutral fragments. If the excitation energy remains localized near the initial excited atom, the chemical bonds around the atom might break easily. Eberhardt and co-workers first observed site-specific fragmen-

tation upon core excitation.[11,12] Selective bond breaking after an excitation of an inner-shell electron of a chosen atom has received increasing attention. Specific dissociation following core-level excitation has been observed for molecules on surfaces and in the gas phase.[13−15] For instance, Baba and co-workers observed Cl$^+$ as the dominant product following excitation of a core electron of the Cl atom in SiCl$_4$ in a condensed phase. When one core electron of a carbon or oxygen atom in Si(OCH$_3$)$_4$ was excited, CH$_3^+$ was the dominant ionic product.[16,17]

We recently studied the core excitation of phenol at both the carbon and oxygen K-edges. Fragments generated from bond-specific dissociation were observed. In particular, O−H bond cleavage was clearly observed only at the oxygen K-edge. As the molecular size increases, vibrational energy redistribution becomes important. It is interesting to investigate the competition between energy redistribution and bond-specific dissociation in larger molecules. In the current study, we investigated the core excitations of phenyl ether at the carbon K-edge and 1,3-diphenoxybenzene at both the carbon and oxygen K-edges. We recorded NEXAFS spectra and mass

spectra of the ionic products formed following Auger decay. Quantum-chemical calculations of the NEXAFS spectra for both the oxygen and carbon K-edges were also performed. The calculated and experimental spectra were compared to elucidate the nature of the various core–electron transitions. From the experimental profiles of ionic products as a function of photon energy, we identified specific dissociations following core-level excitation at specific photon energies. The size effects from the results of the three molecules—phenol, phenyl ether, and 1,3-diphenoxybenzene—were also discussed.

■ EXPERIMENTAL SECTION

The experiment has been described elsewhere,[18] and thus, only brief details and variations from the reported procedures are presented here. An orthogonal acceleration reflectron time-of-flight mass spectrometer (OA-R-TOF MS), located at the Taiwan Light Source at the National Synchrotron Radiation Research Center, was utilized to measure the ion signals. The experiments on phenyl ether employed the same setup as in our previous work.[18] A diffusive molecular beam was generated in the source chamber from a sample cell with an orifice with a diameter of 0.15 mm. The sample cell was kept at 355 K, and the pressure of phenyl ether inside the cell was measured as 1.3 Torr. The diffused molecular beam was collimated by a skimmer (diameter 2 mm) located 8 mm downstream from the sample cell before it entered the ionization chamber. The pressures in the source, ionization, and detection chambers during the experiment were 5.7×10^{-6}, 8.6×10^{-7}, and 5.5×10^{-8} Torr, respectively.

Soft X-rays from a synchrotron were directed into the ionization chamber with two bendable refocusing Kirkpatrick–Baez mirrors coated with Au. This beam crossed the diffusive beam of phenyl ether 20 mm downstream from the skimmer. Molecules ionized by X-ray photons dissociated into ionic fragments because of the internal energy remaining after Auger decay; these ionic fragments were collimated with ion lenses when they were pushed into the region of ion acceleration in the mass spectrometer[18–22] in the detection chamber. When this region was filled with the collimated ions, a pulsed voltage was applied to drive these ions into the region of mass analysis. For phenyl ether, the repetition rate of the pulsed voltage was 50 kHz. A rectangular hole (8.8 mm × 40 mm) separated the ionization and detection chambers; its size was designed to ensure that most of collimated ions could pass through it but the pressure in the detection chamber would be $^1/_{10}$ that in the ionization chamber.

Ions were detected with a microchannel plate (MCP) detector (95 mm × 42 mm). The output signal from this detector was amplified and recorded with a time-of-flight multiscaler (FAST ComTec, model P7888, bin width 2 ns). A counting technique was utilized to accumulate the signal; a discrimination level was set to optimize the signal-to-noise ratio. The stated chemical compounds (Sigma-Aldrich, purity 99%) were used without further purification. The sample cell was evacuated before experiments.

These experiments were performed at undulator beamline BL05B1 at the Taiwan Light Source, details of which have been reported previously;[23] only a brief description is presented here. This beamline delivers $>10^{12}$ photons s^{-1} with energies of 60–1400 eV. The relative energy resolution ($E/\Delta E$) is as large as 20 000, depending on the slit widths and the grating. In the current study, the resolution was about 100 meV at the carbon K-edge for phenyl ether and about 50 and 130 meV at the

carbon and oxygen K-edges, respectively, for 1,3-diphenoxybenzene. The beam spot had a size of 0.4 mm × 0.2 mm at the intersection with the diffusive molecular beam. The photon energy was calibrated using absorption spectra of CO_2 for both the carbon K-edge (290.77 eV) and the oxygen K-edge (535.4 eV).[24–30] The scanning step was 150 meV, and the actual energy resolution in the spectrum was larger than 150 meV.

The experimental conditions for 1,3-diphenoxybenzene differed slightly from those for phenyl ether. Because the vapor pressure is very low (estimated to be less than 0.1 mTorr), the sample cell containing 1,3-diphenoxybenzene was kept at room temperature and directly loaded into the ionization chamber. The exit port of the sample cell (2 mm × 8 mm) was located 2 mm below the path of the synchrotron radiation. The pressures were 4.1×10^{-7} Torr in the ionization chamber and 4.8×10^{-8} Torr in the detection chamber; the repetition rate of the pulsed voltage was 40 kHz.

Both phenyl ether and 1,3-diphenoxybenzene are very sticky molecules and not easy to remove. For each compound, we used a completely new sample cell to avoid contamination. The surface inside the vacuum chamber was wiped with methanol, but contamination was still observed by mass spectrometry for about 2 months. We waited until the contamination completely disappeared before we started the next experiment.

■ COMPUTATIONAL DETAILS

The molecular structures of phenyl ether and 1,3-diphenoxybenzene in their ground electronic states were calculated using the B3LYP hybrid density functional with the 6-311+G(d,p) basis set. Various theoretical methods for calculating NEXAFS spectra with varied degrees of approximations have been reported.[31–42] The multiple-scattering Xα method[31] and the direct static exchange (STEX) method[33,35,43] were highly approximate in nature. Their limitations were due to the neglect of electron-correlation energy and the adoption of an independent-channel approximation. Slater improved the STEX approach to obtain the transition-potential method,[34,35] in which the orbital binding energies are computed as the derivatives of the total energy with respect to the orbital occupation numbers. The excitation energies obtained were typically too small, and the errors mainly arose from the higher-order contributions to the core relaxation energies. In the current study, we adopted time-dependent density functional theory (TDDFT)[44–47] to calculate the carbon and oxygen K-edge NEXAFS spectra of phenol, phenyl ether, and 1,3-diphenoxybenzene. The core-excitation calculation was performed within the subspace of single excitations involving excitations from core orbitals with the Tamm–Dancoff approximation[48] without relativistic corrections. Stener and co-workers[49–51] showed this approach to be satisfactory for X-ray absorption spectroscopy using the LB94 functional,[46,52,53] which produced reasonable results and had the correct asymptotic behaviors. We used the standard Pople-type 6-31+G(d,p) basis set in the calculations with the LB94 functional. The Dunning-type aug-cc-pCVTZ basis set[54–57] containing s- and p-type core polarization functions in addition to the valence triple-ζ basis set and diffuse functions was also used for phenol and phenyl ether to assess the effect of the basis set size. Molecular geometry calculations were performed using the Gaussian 09 program,[58] and the TDDFT calculations for the NEXAFS spectra were performed with the Q-CHEM 4.1 program.[59]

■ RESULTS

A. Calculated and Experimental NEXAFS Spectra. The NEXAFS spectrum of phenyl ether at the carbon K-edge from 284.3 to 298.2 eV in the total ion yield (TIY) mode is shown in Figure 1a, and the corresponding spectra of 1,3-diphenox-
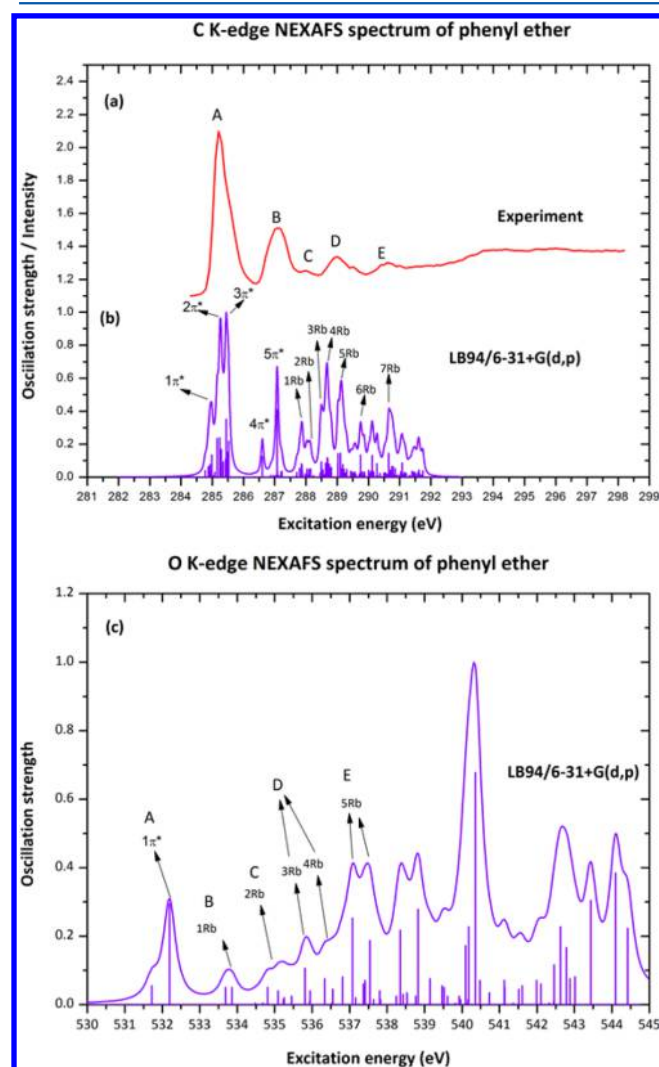
Figure 1. (a) Experimental NEXAFS spectrum in TIY mode (intensity) at the carbon K-edge for phenyl ether excited from 284.3 to 298.2 eV. (b) Calculated carbon K-edge NEXAFS spectrum (oscillation strength) of phenyl ether at the LB94/6-31+G(d,p) level without an energy shift; the line spectrum was convoluted with a Lorentz function having a half-width of 50 meV. (c) Calculated oxygen K-edge NEXAFS spectrum (oscillation strength) of phenyl ether at the LB94/6-31+G(d,p) level without an energy shift; the line spectrum was convoluted with a Lorentz function having a half-width of 200 meV.

ybenzene at the carbon and oxygen K-edges are shown in Figure 2a,c, respectively. The measured signal-to-noise ratio of the NEXAFS spectrum of phenyl ether at the oxygen K-edge was poor, and thus, that spectrum is not presented in this article.

Figure 3 shows the calculated molecular geometries of phenyl ether and 1,3-diphenoxybenzene. Two conformers of 1,3-diphenoxybenzene having similar energies and structures were found. The energy of the conformer with C_s symmetry was predicted to be 0.2 kcal/mol lower at the M06-2X[60]/6-
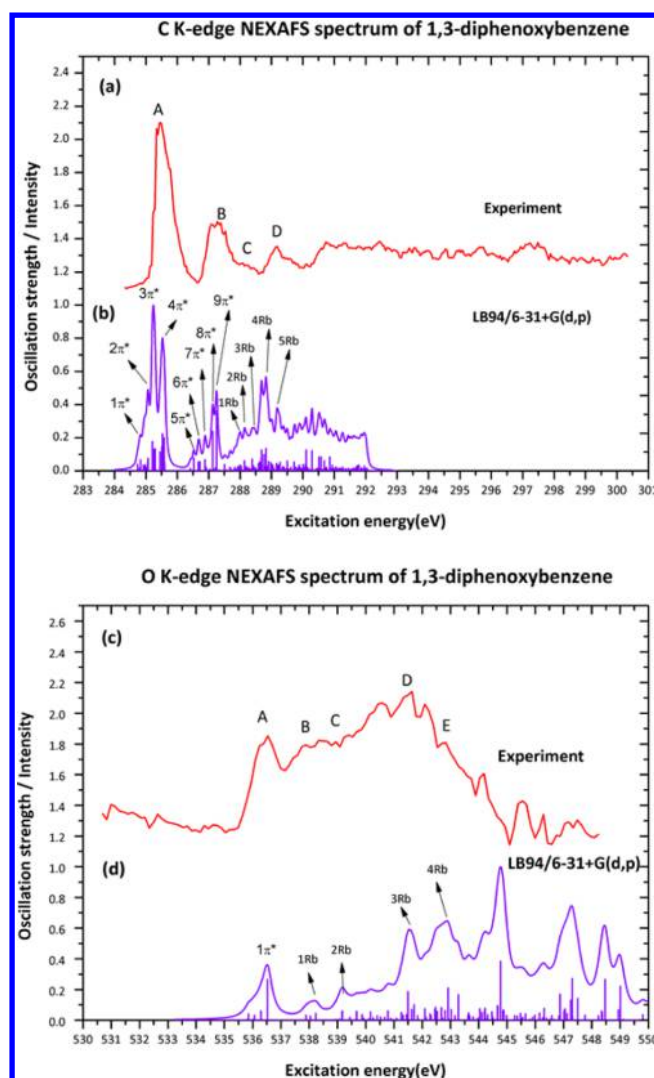
Figure 2. (a) Experimental NEXAFS spectra in the TIY mode (intensity) at the carbon K-edge for 1,3-diphenoxybenzene excited from 284.3 to 298.2 eV. (b) Calculated carbon K-edge NEXAFS spectrum (oscillation strength) of 1,3-diphenoxybenzene at the LB94/6-31+G(d,p) level without an energy shift. The line spectrum was convoluted with a Lorentz function having a half-width of 50 meV. (c) Experimental NEXAFS spectrum (intensity) at the oxygen K-edge for 1,3-diphenoxybenzene (measured with an energy resolution of 130 meV). (d) Calculated oxygen K-edge NEXAFS spectrum (oscillation strength) of 1,3-diphenoxybenzene at the LB94/6-31+G(d,p) level with an energy shift of +4.24 eV; the line spectrum was convoluted with a Lorentz function having a half-width of 200 meV.

311+G(d,p) level. As the current TDDFT approximation did not take into account the electronic states in the continuum, the calculated transitions at lower energies would be more reliable and more meaningful in comparison to the experimental spectra. The NEXAFS spectra calculated with the 6-31+G(d,p) and aug-cc-pCVTZ basis sets were qualitatively similar. However, the spectra calculated with the latter basis set required significantly larger energy shifts to match the experimental spectra satisfactorily. The following discussion is hence based on the LB94/6-31+G(d,p) results. (The spectra of phenol and phenyl ether calculated using the aug-cc-pCVTZ basis set are shown in Figures S1 and S2 in the Supporting Information for comparison.) Figure 1b shows the calculated carbon K-edge NEXAFS spectrum of phenyl ether.
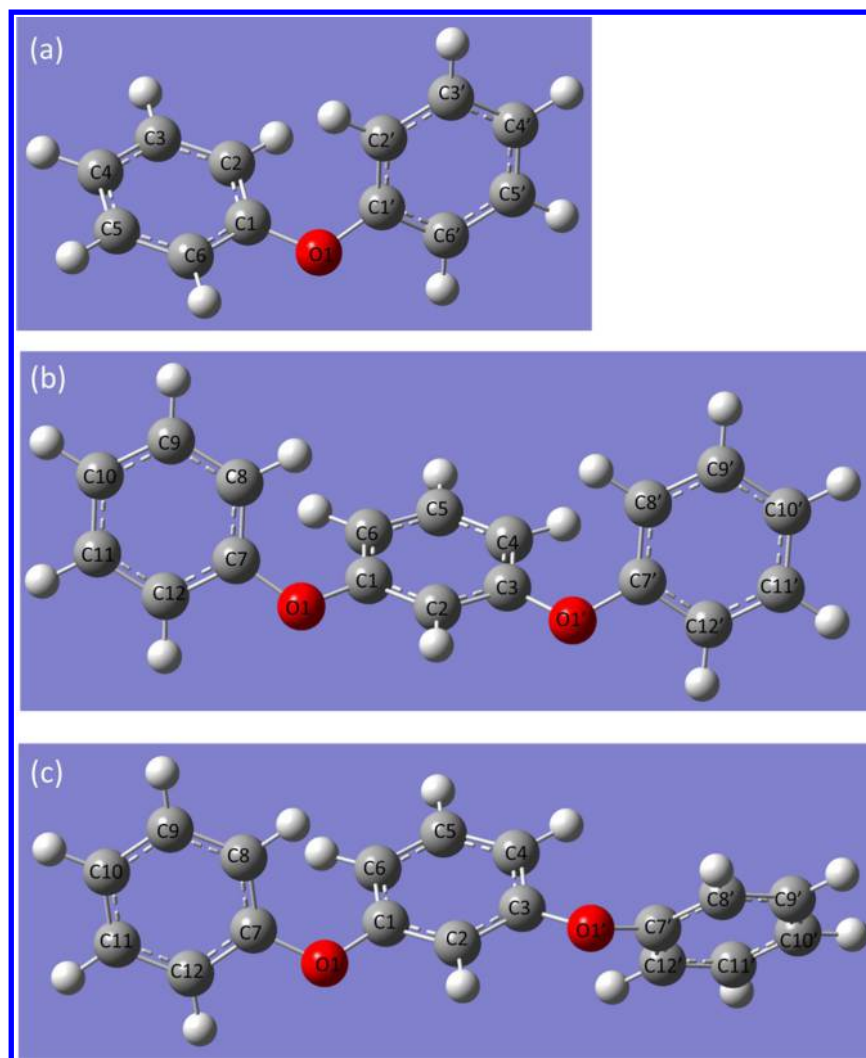
7805

dx.doi.org/10.1021/jp505949d | J. Phys. Chem. A 2014, 118, 7803−7815

Figure 3. Calculated structures at the B3LYP/6-311+G(d,p) level: (a) phenyl ether; (b) 1,3-diphenoxybenzene with C_s symmetry; (c) 1,3-diphenoxybenzene with C_1 symmetry.

Table 1. Assignment of the NEXAFS Spectrum of Phenyl Ether at the C K-Edge[a]

			excitation energy/eV	
area	peak	resonance	LB94/6-31+G(d,p)	exptl
A	$1\pi^*$	C**2,2',4,4',5,5',6,6'** → π^* (V1, V2)	284.9	285.2
	$2\pi^*$	C**2,2'**,3,3',**5,5',6,6'** → π^* (V3)	285.3	285.2
	$3\pi^*$	C**2,2',3,3',4,4'**,5,5' → π^* (V4)	285.4	285.2
B	$4\pi^*$	C**1,1'** → π^* (V2)	286.6	287.1
	$5\pi^*$	C**1,1'** → π^* (V4)	287.1	287.1
C	1Rb	C**2,2',3,3',4,4',5,5'** → Rydberg (minor σ^*, V8, V9)	287.8	288.0
C	2Rb	C**2,2',4,4',6,6'** → Rydberg (V10, V11, V12)	288.1	288.0
D	3Rb	C**4,4',6,6'** → Rydberg (V13, V14)	288.5	289.0
	4Rb	C**3,3',4,4',6,6',11,11'** → Rydberg (V12, V15)	288.7	289.0
	5Rb	C**2,2',3,3',4,4',5,5',6,6'** → Rydberg (V16, V18)	289.1	289.0
	6Rb	C**1,1',2,2',4,4',6,6'** → Rydberg (V21, V22)	289.7	289.5
E	7Rb	C**1,1',2,2',6,6'** → Rydberg (V18, V28)	290.7	290.6

[a]The resonance C1,1' → π^* (V2) signifies that the 1s electron on carbon 1 or 1' in phenyl ether is excited to a π^* orbital as the second virtual (unoccupied) orbital. The atoms making the major contributions are labeled in italics. See Figure 3 for atom labeling. The calculated excitation energies are unshifted.

As the calculated NEXAFS spectra of two conformers of 1,3-diphenoxybenzene were almost identical, only that of the conformer with C_s symmetry is shown in Figure 2b. Tables 1 and 2 present the assignments of the absorption peaks. The core-excited carbon atoms and the destination virtual orbitals (labeled Vn) for the major transitions are indicated in these tables. Some of the transition orbitals of phenyl ether are presented in Figure 4, and some of the transition orbitals of 1,3-

Table 2. Assignment of the NEXAFS Spectrum of 1,3-Diphenoxybenzene (C_s Symmetry) at the C K-Edge[a]

			excitation energy/eV	
area	peak	resonance	LB94/6-31+G(d,p)	exptl
A	1π*	C**4,6,10,10′,12,12′** → π* (V1, V2)	284.8	285.4
	2π*	C4,5,6,**10,10′,12,12′** → π* (V3, V4)	285.1	285.4
	3π*	C2,4,6,**8,8′**,9,9′,10,10′,**11,11′**,12,12′ → π* (V4, V5)	285.2	285.4
	4π*	C**4,5,6**,8,8′,9,9′,**10,10′**,11,11′ → π* (V5, V6)	285.5	285.4
B	5π*	C**1,3**,7,7′ → π* (V2)	286.5	287.3
	6π*	C1,3,7,7′ → π* (V4)	286.7	287.3
	7π*	C7,7′ → π* (V5)	286.9	287.3
	8π*	C7,7′ → π* (V6, V8)	287.1	287.3
	9π*	C**1,3**,4,6,9,9′ → π* (V6,9)	287.2	287.3
C	1Rb	C**4,6,9,9′,11,11′** → Rydberg (minor σ*, V11, V13, V14)	287.8	288.0
	2Rb	C2,4,6,**10,10′,12,12′** → Rydberg (minor σ*, V15, V16)	288.1	288.0
	3Rb	C**4,6,9,9′**,10,10′,11,11′ → Rydberg (V18, V19)	288.8	288.0
D	4Rb	C4,5,6,**8,8′,9,9′**,10,10′,**11,11′**,12,12′ → Rydberg (V18, V19, V21)	288.9	289.2
	5Rb	C2,4,5,6,8,8′,**10,10′,12,12′** → Rydberg (V20, V21)	289.2	289.2

[a]The resonance C7,7′ → π* (V5) signifies that the 1s electron on carbon 7 or 7′ in 1,3-diphenoxybenzene is excited to a π* orbital as the fifth virtual (unoccupied) orbital. The atoms making the major contributions are labeled in italics. See Figure 3 for atom labeling. The calculated excitation energies are unshifted.

diphenoxybenzene are presented in Figure 5; others are shown in Figures S3−S6 in the Supporting Information.

The calculated carbon K-edge NEXAFS spectra of phenyl ether and 1,3-diphenoxybenzene are roughly divisible into three areas, designated as low-, moderate- and high-energy areas. All of the transitions in the low-energy area (group A in Figures 1a
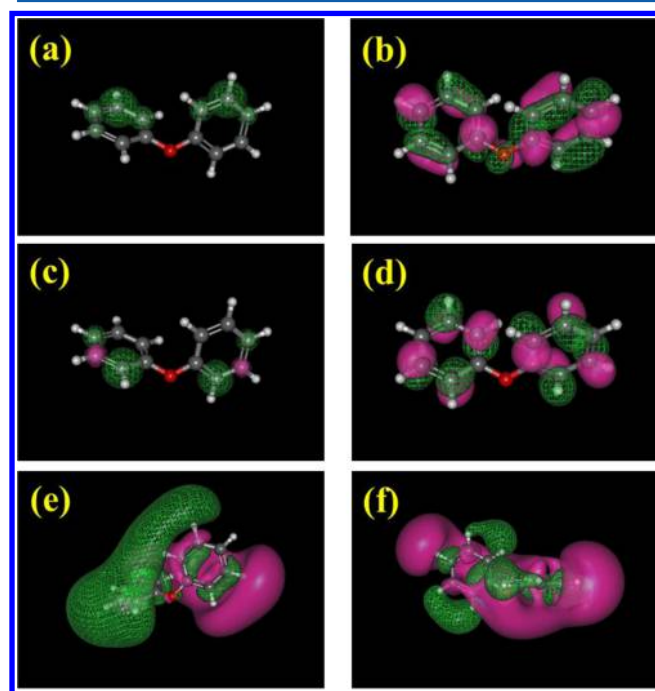

Figure 4. Calculated core-excitation transition orbitals for the carbon K-edge NEXAFS spectrum of phenyl ether. The core orbitals shown in (a) and (c) are linear combinations of 1s orbitals localized on carbons not directly bound to oxygen; the destination orbitals shown in (b) and (d) are delocalized π* orbitals on both phenyl rings. The transitions (a) → (b) and (c) → (d) correspond to the two highest signals in area A (2π* and 3π*, respectively) in Figure 1b. Panels (e) and (f) show the destination orbitals with minor σ* character along C−H bonds for the transitions to 1Rb and 2Rb, respectively, in area C of Figure 1b.
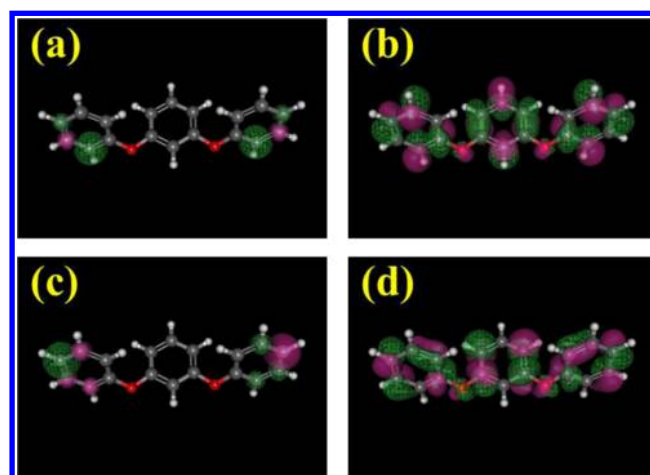

Figure 5. Calculated core-excitation orbitals of the carbon K-edge NEXAFS spectrum of 1,3-diphenoxybenzene. Transitions (a) → (b) and (c) → (d) correspond to the two strongest transitions, labeled as 3π* and 4π* in Figure 2b. The core orbitals shown in (a) and (c) are carbon 1s orbitals localized on the various carbons; the destination orbitals shown in (b) and (d) are delocalized π* orbitals on the benzene rings.

and 2a) were predicted to be of the type 1s → π*. As shown in Figure 4a−d and Figures 5, the starting 1s orbitals are localized on carbon atoms *not* directly bonded to the oxygen atom, and the destination π* orbitals are delocalized over the phenyl rings. The transitions in the moderate-energy area (groups B and C in Figures 1a and 2a) were predicted to involve 1s → π* and 1s → Rydberg states. For the 1s → π* transitions in this area, the initial 1s orbitals are localized on the carbon atoms directly bonded to the oxygen atom. Most of the destination orbitals of symmetry other than π* in the moderate-energy area were predicted to be diffuse (Rydberg) orbitals with only minor σ* character. The transitions in the high-energy area (groups D and E in the NEXAFS spectra at the carbon K-edge) were predicted to be only of the type 1s → Rydberg states. With a transition-potential approach, Pettersson[61] assigned some signals in this area as 1s → σ*. We found some destination orbitals in this area that contain minor σ* character, and they

Table 3. Assignment of the NEXAFS Spectrum of Phenyl Ether at the O K-Edge[a]

area	peak	resonance	LB94/6-31+G(d,p) excitation energy/eV
A	$1\pi^*$	$O1 \to \pi^*$ (V2, V4)	532.2
B	1Rb	$O1 \to$ Rydberg (minor σ^*, V5, V6)	533.7
C	2Rb	$O1 \to$ Rydberg (minor σ^*, V11, V14)	535.1
D	3Rb	$O1 \to$ Rydberg (V16, V17)	535.8
D	4Rb	$O1 \to$ Rydberg (V19, V21)	536.8
E	5Rb	$O1 \to$ Rydberg (V27, V28)	537.3

[a]The resonance $O1 \to \pi^*$ (V2, V4) signifies that the 1s electron on the oxygen atom in phenyl ether is excited to two π^* orbitals as the second and fourth virtual orbitals. The calculated excitation energies are unshifted.

Table 4. Assignment of the NEXAFS Spectrum of 1,3-Diphenoxybenzene (C_s Symmetry) at the O K-Edge[a]

area	peak	resonance	excitation energy/eV	
			LB94/6-31+G(d,p)	exptl
A	$1\pi^*$	$O1,1' \to \pi^*$ (V2, V4, V5, V6)	536.5	536.5
B	1Rb	$O1,1' \to$ Rydberg (minor σ^*, V8, V9)	538.1	537.9
C	2Rb	$O1,1' \to$ Rydberg (minor σ^*, V15, V16)	539.1	538.9
D	3Rb	$O1,1' \to$ Rydberg (V36, V38)	541.5	541.5
E	4Rb	$O1,1' \to$ Rydberg (V53, V57)	542.8	543.0

[a]The resonance $O1,1' \to \pi^*$ (V2, V4, V5, V6) signifies that the 1s electron on O1 or O1' in 1,3-diphenoxybenzene is excited to four π^* orbitals as the second, fourth, fifth, and sixth virtual orbitals. The calculated excitation energies are shifted by 4.24 eV.

are shown in Figure 4e,f and Figure S4-3b in the Supporting Information.

Figures 1c and 2d show the calculated oxygen K-edge NEXAFS spectra of phenyl ether and 1,3-diphenoxybenzene. The calculated oxygen NEXAFS spectra can similarly be divided into three areas. The assignments of the absorption peaks are shown in Tables 3 and 4. Two sets of destination orbitals of phenyl ether were identical to those presented in Figure 4b,d, and two sets of destination orbitals of 1,3-diphenoxybenzne were identical to those presented in Figure 5b,d; others are included in Figures S5 and S6 in the Supporting Information. For phenyl ether, the transitions in the low-energy area (group A) were found to be of the type oxygen 1s → π^*, in which the destination π^* orbitals are delocalized over both phenyl rings as shown in Figure 4b,d. All of the other peaks were found to correspond to oxygen 1s → Rydberg state transitions. For 1,3-diphenoxybenzene, the transitions in the low-energy area (group A) were found to be of the type oxygen 1s → π^*, in which the destination π^* orbitals were delocalized over the three benzene rings as shown in Figure 5b,d. All of the other peaks were found to correspond to oxygen 1s → Rydberg state transitions (see Figures S5 and S6 in the Supporting Information.) For comparison, the analysis of the NEXAFS spectra of phenol is shown in the Supporting Information (see Figures S7−S9 and Tables S1 and S2.) The assignments are very similar to those for phenyl ether and 1,3-diphenoxybenzene. That is, in the carbon K-edge spectrum, the low-energy 1s → π^* transitions originate from the carbon atoms not directly bonded to the oxygen atom, and the moderate-energy 1s → π^* transitions originate from the carbon atoms directly bonded to the oxygen atom; the high-energy peaks were assigned as 1s → Rydberg states. In the oxygen K-edge spectrum, the low-energy peak was assigned as a 1s → π^* transition, and other peaks were assigned as 1s → Rydberg state transitions.

Both the calculated carbon and oxygen K-edge spectra of phenyl ether and 1,3-diphenoxybenzene agree satisfactorily with the experimental spectra after only minor energy shifts (from 0.0 to 4.24 eV), which were necessary because of systematic errors of the LB94 functional and the underlying TDDFT approximation. The line widths of the experimental spectra are related to the experimental energy resolution and the lifetimes of the excited states; they cannot be estimated accurately in the current calculations. The vibrational motion of molecules might affect the relative intensities and cause some forbidden transitions to appear in the experimental results. The calculation of the carbon K-edge spectra clearly showed that the difference in the chemical environments of the carbon atoms caused perceptible shifts in the NEXAFS spectra. For phenol, phenyl ether, and 1,3-diphenoxybenzene, the core excitations to the π^* orbitals of the carbon atoms bonded directly to the oxygen atoms are approximately 2 eV higher in energy than the core excitations of other carbon atoms.

B. Dissociation of Phenyl Ether. Figure 6 shows mass spectra of phenyl ether excited at various photon energies at the carbon K-edge. The major ionic products following core excitation and Auger decay show peaks at m/z = 39, 50, 51, 63, 65, 74, 77, 115, 139, and 141 u. The mass spectra at various excitation energies are similar, although the relative intensities of the ions vary. For example, the relative intensities of parent ion (m/z = 170 u) and the ionic products (m/z = 141 and 77 u) are high at photon energies of 285.2 and 287.1 eV but small at photon energies higher than 288 eV. The ionic product with m/z = 50 u has the highest intensity only for photon energies lower than 290.6 eV. The intensity of the ionic product with m/z = 39 u becomes the highest for photon energies beyond 290.6 eV.

Figure 7a shows the ion intensities as a function of photon energy for each major product ion. One clear feature shown therein is the high intensity of absorption lines centered at 285.2, 287.1, and 289 eV. Another feature is the high intensity for small product ions (e.g., those with m/z = 27, 39, 50, 63, 65, and 74 u) at photon energies higher than 290 eV. To seek possible dissociations specific to a bond or site following core excitation and Auger decay, we plotted the intensity ratios (defined as the intensity of each ion divided by the total ion intensity at the same photon energy) of major product ions as a function of photon energy (Figure 7b).
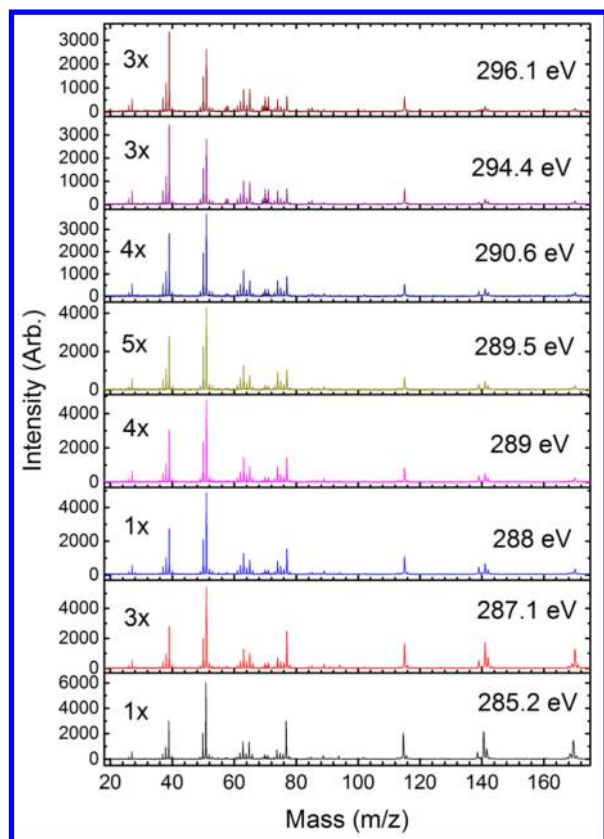
Figure 6. Mass spectra of the dissociation of phenyl ether following core excitation and Auger decay. These excitation energies were chosen according to the absorption lines or broad lines in the carbon NEXAFS spectrum of phenyl ether (Figure 1a). To obtain similar signal-to-noise ratios, the periods of integration were varied as noted in each mass spectrum.

The intensity ratio of parent ions (with m/z = 170 u) shows two lines located at 285.2 and 287.1 eV, representing a high probability that the ionization was not followed by fractionation or ejection of a second electron. These two lines correspond to

the excitations 1s → π^* of C2−C6 and C2′−C6′ and 1s → π^* of C1 and C1′, respectively, followed by an ejection of an Auger electron carrying away most of the energy. The energy left for phenyl ether cations was so small that dissociation or ejection of a second electron did not occur, resulting in parent ions. The probability of producing singly charged parent ions was low for photon energies higher than the direct ionization threshold (about 290 eV). When the photon energy exceeded the direct threshold of ionization, the first electron was ejected upon radiative excitation. The ejection of a second electron occurred after the Auger decay, resulting in doubly charged parent ions. Most of the doubly charged parent ions dissociated into smaller ionic fragments, and only a small fraction remained without fractionation, resulting in ions with m/z = 85 u.

The intensity ratio of the ion with m/z = 141 u shows features similar to those of the parent ions. The ionic product with m/z = 141 u is greatly enhanced at photon energies of 285.2 and 287.1 eV. Possible compositions for m/z = 141 u are $C_{10}H_5O^+$ and $C_{11}H_9^+$. The ionic fragment $C_{10}H_5O^+$ can be produced by breaking two C−C bonds in one aromatic ring, eliminating C_2H_2 with three additional H atoms or eliminating C_2H_4 and one H atom. Another possible path involves the removal of CH from each aromatic ring with an additional three hydrogen atoms. The other possible composition of an ion with m/z = 141 u is $C_{11}H_9^+$, which might be produced from the elimination of CHO (or CO and H). Elimination of C_2H_2 or C_2H_4 is a major dissociation channel of the benzene cation;[62,63] elimination of CO is a major dissociation channel of the phenol cation,[63−65] but extensive isomerization (e.g., fusion of two aromatic rings) is required before this elimination can occur. An ionic fragment with m/z = 139 u might result from elimination of an additional two H atoms from a fragment with m/z = 141 u. The possible formulas and bond cleavages of most of the major ionic products are organized in Table S3 in Supporting Information.

The ions with m/z = 115 u are also greatly enhanced at photon energies of 285.2 and 287.1 eV. This ionic product has two possible compositions: $C_8H_3O^+$ and $C_9H_7^+$. The ionic product $C_8H_3O^+$ might be produced by the elimination of four

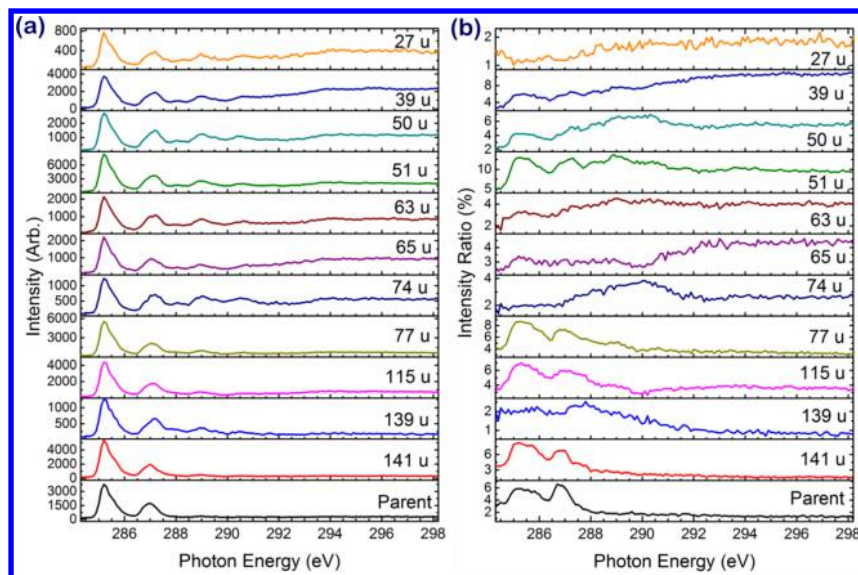**Figure 7.** (a) Intensities of major product ions produced upon excitation of core electrons in carbon atoms of phenyl ether. The ratio of mass to charge is indicated in each figure. (b) Intensity ratios (as percentages) of major ionic products.

sets of fragments: C_4H_4 with three additional hydrogen atoms; two C_2H_2 fragments with three additional hydrogen atoms; C_2H_4, C_2H_2, and one H atom; and CH_3, C_3H_3, and one H atom. Eliminations of C_4H_4, C_2H_4, C_2H_2, C_3H_3, and CH_3 are all major dissociation channels of the benzene cation.[62,63] The other possible composition of an ion with $m/z = 115$ u, $C_9H_7^+$, would require an elimination of fragments that contain an oxygen atom; the possible fragments include CO, C_2H_2, and one H atom. As mentioned above, an elimination of CO must involve extensive isomerization.

Another major ionic product, with $m/z = 77$ u, likely is the phenyl radical cation, $C_6H_5^+$, which is commonly associated with the dissociation of an aromatic cation.[66] The generation of $C_6H_5^+$ requires cleavage of the C−O bond. The formation of $C_6H_5^+$ is clearly enhanced following C 1s → π^* excitation from any carbon atom.

Other major products are ions with small m/z values, including 65, 63, 51, 50, 39, and 27 u. These ions are also major products of phenol cations following core excitation.[18] The possible compositions with $m/z = 65$ and 63 u are $C_5H_5^+$ and $C_5H_3^+$, respectively, which might be produced from a path analogous to the elimination of CO from the phenol cation with additional elimination of H atoms. Another possible composition with $m/z = 65$ u is C_4HO^+, which would result from elimination of C_2H_2 and H atoms. The possible compositions with $m/z = 51$, 50, 39, and 27 u are $C_4H_3^+$, $C_4H_2^+$, $C_3H_3^+$, and $C_2H_3^+$, respectively, which can be produced from paths analogous to the dissociation paths of the benzene cation that generate $C_4H_4^+$, $C_4H_3^+$, $C_4H_2^+$, and $C_3H_3^+$.[62] Most of the intensities are greatly enhanced for photon energies higher than the ionization threshold, indicating production from doubly charged phenyl ether cations. One possible explanation is that singly charged phenyl ether cations produced only fragments with charge located mainly on the larger fragment, such as those with $m/z = 141$ and 115 u. Charges are located on both small and large fragments when the parent ions are doubly charged.

C. Dissociation of 1,3-Diphenoxybenzene. Figure 8 shows the mass spectra of 1,3-diphenoxybenzene at the resonance excitation energies at the carbon K-edge. The major ionic products include those with $m/z = 39$, 51, 63, 77, 115, 128, 139, 141, 168, and 262 u (parent ions). The major ions at various photon energies remain the same, but the relative intensities vary. For example, ions with $m/z = 77$, 115, 139, 141, and 168 u and parent ions are the dominant products for the transition 1s → π^* (285.44 or 287.29 eV). As the photon energy increases and the core electron become excited to Rydberg states, the intensities of heavier ionic fragments with $m/z = 115$, 139, 141, and 168 u and the parent ions decrease significantly. Smaller ionic fragments with $m/z = 77$ and 51 u become the dominant products at higher energies.

Figure 9 shows the intensity (panel a) and intensity ratio (panel b) as functions of photon energy for major ionic products. Unlike for phenol and phenyl ether, the enhancement of the ion intensity ratio at resonance excitation energies of 285.44 and 287.29 eV was not evident. Smoother ion intensity ratio curves that varied slowly with photon energy were observed instead. The enhancement of the ion intensity ratio is divisible approximately into three regions: (1) 1s → π^* (lower-energy region, below 288 eV), (2) 1s → Rydberg states (region of moderate energy, between 288 and 291 eV), and (3) 1s → above C 1s [i.e., beyond the ionization energy of C 1s (291 eV)]. The parent ion and ionic fragments with $m/z = 141$ and
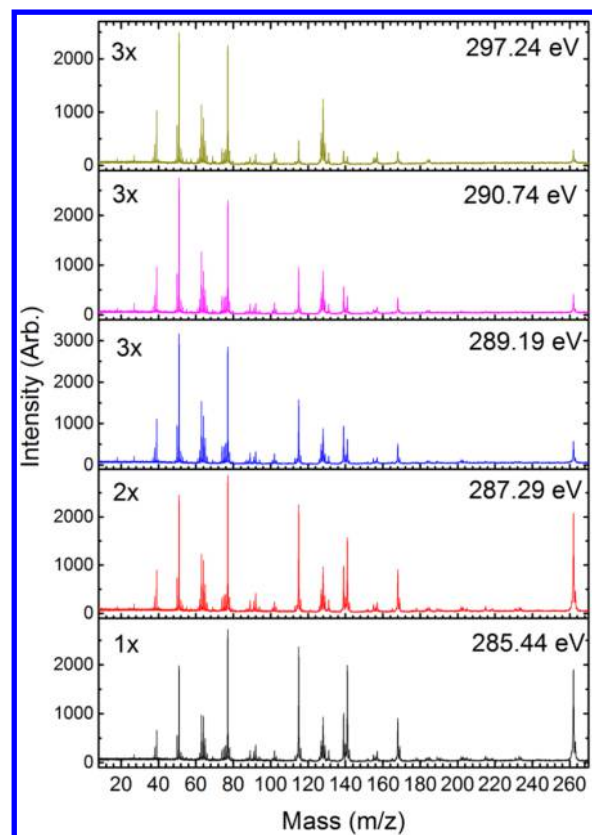

Figure 8. Mass spectra of 1,3-diphenoxybenzene dissociation upon core excitation and Auger decay. These excitation energies were chosen according to the absorption lines or broad lines in the carbon NEXAFS spectrum of 1,3-diphenoxybenzene (Figure 2a).

168 u showed high ion intensity ratios only in the first region; the ionic fragments with $m/z = 115$ and 139 u showed high ion intensity ratios in the first and second regions. Most of the small fragment ions (with $m/z = 39$, 50, 51, 63, 64, and 77 u) showed high ion intensity ratios in the second and third regions. Three ionic products, with $m/z = 127$, 128, and 157 u, were enhanced significantly only in the third region.

Because most of the ionic products (with $m/z = 39$, 51, 63, 77, 115, 139, and 141 u) have the same mass-to-charge ratio as those of phenyl ether, the possible compositions of these products are not repeated here. The dissociation mechanism may not be the same. For example, the intensity ratio curve of the ion with $m/z = 139$ u produced from 1,3-diphenoxybenzene is similar to that from phenyl ether, indicating that the dissociation pathways may be similar. On the other hand, the curves for the ion with $m/z = 77$ u are totally different for phenyl ether and 1,3-diphenoxybenzene, indicating that the dissociation pathways are very different. The ionic fragments with $m/z = 262$, 168, 157, 128, and 127 u were not observed in phenyl ether. Their compositions and dissociation pathways are further discussed in the following paragraphs.

Similar to phenyl ether, the ion intensity ratio of the singly charged parent ion of 1,3-diphenoxybenzene ($m/z = 262$ u) is high only in the region of low energy (1s → π^* transition). As the photon energy increased, most of the singly charged parent ions dissociated into smaller fragments or became doubly charged parent ions. The relative ion intensities of $m/z = 131$ and 131.5 u are close to the natural abundances of the ^{12}C and ^{13}C isotopes. Therefore, we assigned ion with $m/z = 131$ u as
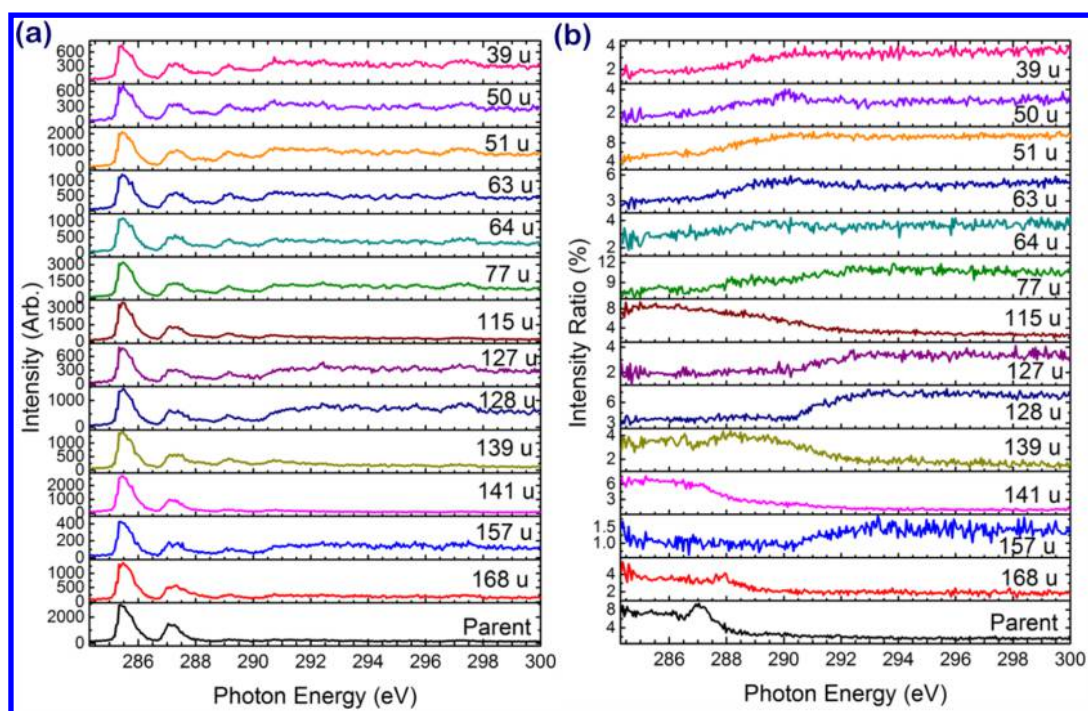
Figure 9. (a) Intensities of major ionic products produced upon excitation of core electrons of carbon atoms in 1,3-diphenoxybenzene. The ratio of mass to charge is indicated in each figure. (b) Intensity ratios (as percentages) of major ionic products.

Figure 10. (a) Intensities of major ionic products produced upon excitation of core electrons of oxygen atoms in 1,3-diphenoxybenzene. The ratio of mass to charge is indicated in each figure. (b) Intensity ratios (as percentages) of major ionic products.
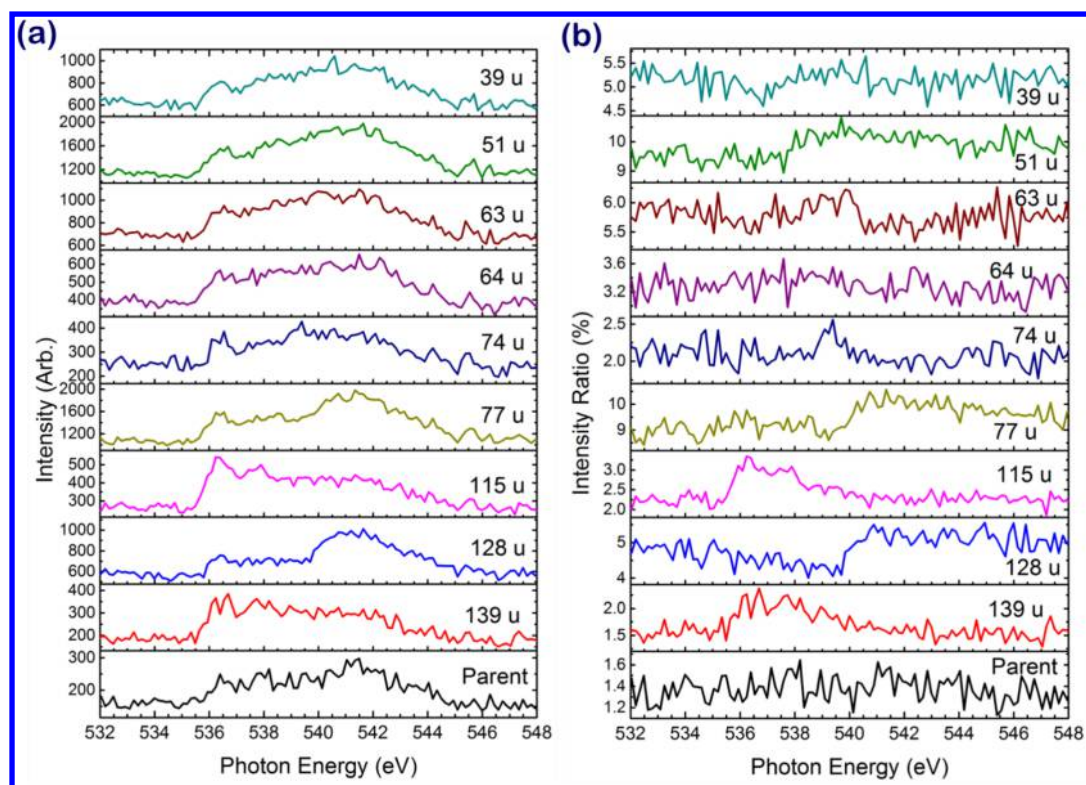
the doubly charged parent ion. Unlike the case of phenol, for which doubly charged parent ions were observed more in regions of moderate and high energy, the intensity ratios of the doubly charged parent ion (m/z = 131 u) remain near 1% in all three energy regions.

The possible compositions of a fragment with m/z = 169 u include $C_{12}H_9O^+$ and $C_{11}H_5O_2^+$. The ionic fragment $C_{12}H_8O^+$ is produced from the elimination of C_6H_5O upon cleavage of the C−O bond. The elimination of an additional H atom produces an ionic fragment with m/z = 168 u. The intensity ratio curve for $C_{12}H_9O^+$ (m/z = 169 u) is almost identical to

that of $C_{12}H_8O^+$ (m/z = 168 u). Although these two fragments, $C_{12}H_9O^+$ and $C_{12}H_8O^+$, result from cleavage of the C1−O1 or C3−O1′ bond, no clear enhancement from the excitation of C1 or C3 at 287.29 eV was observed. The other possible composition with m/z = 169 u is $C_{11}H_5O_2^+$. The probability of this composition is low because extensive cleavage of chemical bonds and isomerization would be required.

The possible compositions of the fragment with m/z = 157 u are $C_{11}H_9O^+$ and $C_{10}H_5O_2^+$. Cleavage of C7−O1 or C7′−O1′ (elimination of C_6H_5) followed by elimination of CO could readily generate the $C_{11}H_9O^+$ fragment, but no clear enhancement from the excitation of C7 or C7′ at 287.29 eV was observed. The other composition is unlikely because extensive cleavage of bonds and isomerization would be required. The intensity curve of the fragment with m/z = 157 u in Figure 9b is almost the same as that of the product with m/z = 65 u from phenyl ether in Figure 7b. The dissociation mechanisms for these two ions are very possibly similar, so $C_{11}H_9O^+$ is proposed as the formula of this ionic product.

The ion intensity ratio curves for the fragments with m/z = 127 and 128 u are identical, indicating that they were produced in the same dissociation channel. The possible compositions with m/z = 127 and 128 u are $C_9H_3O^+$ and $C_9H_4O^+$ or $C_{10}H_7^+$ and $C_{10}H_8^+$. $C_9H_4O^+$ can be generated by breaking the parent molecule in half to produce $C_9OH_7^+$, followed by additional elimination of H atoms. The most stable structure of the other possible composition, $C_{10}H_8^+$, is the naphthalene cation; its generation would require the fusion of two aromatic rings and the elimination of an oxygen atom connecting two aromatic rings. This channel is enhanced in only the region of high photon energy; it is unrelated to excitations of specific carbon atoms.

One interesting observation is the relative ion intensity of m/z = 50 and 51 u. The relative ion intensity is 2:1 (m/z = 50 u to m/z = 51 u) in phenol. The ratio changes to 1:2−1:3 in phenyl ether and becomes 1:3 or 1:4 in 1,3-diphenoxybenzene. The trend shows that additional H atom elimination from ionic fragments occurs easily for small-sized molecules. It is likely that the available energy is distributed over the entire molecule. Additional H atom elimination is slow for large-sized molecules because of the large number of vibrational degrees of freedom.

Figure S10 in the Supporting Information shows mass spectra at resonant excitation energies of oxygen K-edge excitation; the major ionic fragments are the same as those for excitation at the carbon K-edge. The relative intensities are similar to those in the mass spectra with carbon K-edge excitation in the region of high energy (>290 eV): for example, the intensities of ionic fragments with high masses and parent ions are small. One major difference between the mass spectra with C K-edge and O K-edge excitations is the relative intensities of ions with m/z = 115, 139, 141, and 168 u, and parent ions. High relative intensities of these ions were observed only in the region of low energy at the C K-edge; they became minute in the entire O K-edge region.

The ion intensity as a function of photon energy in oxygen K-edge excitation (Figure 10 a) shows that all of the ionic fragments have a broad line between 536 and 545 eV. Some fragments (with m/z = 139, 115, 77, and 74 u) have an additional line located at 536.54 eV. Figure 10b shows the ion intensity ratios for various fragments. The fragments with m/z = 139 and 115 u are much enhanced at an excitation energy corresponding to the 1s → 1π* transition, and fragments with m/z = 128 and 77 u are much enhanced at 1s → 3Rb and 1s →

4Rb transitions, where nRb denotes a Rydberg orbital. No clear enhancement was observed for smaller fragments.

Fragments resulting from cleavage of the C−O bond would be expected to be much enhanced upon excitation at the oxygen K-edge if the dissociation occurred at a specific site. These fragments have m/z = 77 ($C_6H_5^+$), 157 ($C_{11}H_9O^+$), and 169 u ($C_{12}H_9O^+$) according to the possible mechanism of dissociation described above. The intensities of ions with m/z = 157 and 169 u were too small for further consideration. Although the ion intensity ratio for m/z = 77 u was near 10%, which is one of the highest among various fragments upon excitation at the oxygen K-edge, the ratio was near that for m/z = 77 u upon excitation at the carbon K-edge, indicating that no dissociation occurred at a specific site upon excitation at the oxygen K-edge.

■ DISCUSSION

Specific dissociations are generally classified as involving elements and sites. This classification is attributed to the excitation of atoms of different elements and atoms of the same elements in varied chemical environments, respectively.[16] A possible mechanism leading to a specific dissociation is localization of excitation and rapid dissociation following core excitation and Auger decay. If the final state after Auger decay is localized at a specific atom or chemical bond and the dissociation is more rapid than energy redistribution, dissociation is more likely to occur around this excited atom. One example is the excitation to a σ* orbital of a specific chemical bond. If the electron is initially excited from a core orbital to an antibonding orbital, or if it is redistributed to an antibonding orbital after Auger decay, the antibonding characteristic causes rapid dissociation along this chemical bond. In contrast, if the intramolecular redistribution of energy is more rapid than dissociation, the excess energy is distributed among all of the degrees of freedom, resulting in dissociation according to statistical predictions. The branching ratios among various dissociation channels would consequently be expected to vary slowly with the photon energy.

The branching ratios of the products corresponding to dissociation at specific sites or elements are typically small. For example, for 2-, 3-, and 4-methylpyridine, Okada and co-workers found the branching ratios of specific dissociation to be only 1.2−1.9%.[67] For the specific bond dissociation of CH_3COOCD_3 at the O K-edge, Kawasaki et al.[68] found the branching ratio of the product CD_3^+ to increase from 5.9% (with excitation at 535.1 eV) to 12.8% (with excitation at 531.9 eV). For the products of methanol following core excitation at the carbon and oxygen K-edges, Stolte and co-workers found that the anionic product OH⁻ was produced at only the C K-edge while O^{2+} was observed only at the O K-edge. Both OH⁻ and O^{2+} are ionic products for which the branching ratios (not available) vary with photon energy.[69−72] A large branching ratio from dissociation at a specific bond has been observed; for example, the branching ratios of the ionic products Cl⁺ from $SiCl_4$ and CH_3^+ from $Si(OCH_3)_4$ are less than 5% and 20%, respectively, following excitation of a Si core electron but increase to 80% after core excitation of the Cl atom in $SiCl_4$ and the O atom in $Si(OCH_3)_4$.[16,17]

The generation of ionic fragments with m/z = 141, 115, 77, and 51 u from phenyl ether is enhanced at 285.2 and 287.1 eV. The branching ratios increase from 3.7, 3.3, 3.9, and 5.2% to 8.2, 7, 8.7, and 13%, respectively. These two lines correspond mainly to 1s → π* excitation of C2−C6 or C2′−C6′ and 1s →

π^* excitation of C1 or C1′. Fragments with m/z = 141, 115, and 51 u are produced by breaking two C−C bonds in one aromatic ring or by eliminating CHO (or CO and H); they involve the excitation of C2−C6 or C2′−C6′ and C1 or C1′, respectively. The enhancements observed at 285.2 and 287.1 eV are hence reasonable, but the generation of a fragment with m/z = 77 u requires the cleavage of a C−O bond, which is expected to be enhanced only upon 1s → π^* excitation of C1 (at 287.1 eV). The formation of $C_6H_5^+$ is enhanced following excitation of every C atom. The branching ratios increased from 5.2% to 8.7% and 7.3% at 285.2 and 287.1 eV, respectively, contrary to our expectation. This observed enhancement represents a mechanism of specific dissociation, as this channel fails to conform to dissociation at a specific site or for a specific element.[16]

The dissociation properties of 1,3-diphenoxybenzene differ significantly from those of phenol and phenyl ether. Although the ionic products from 1,3-diphenoxybenzene with m/z = 51, 77, 115, and 141 u are the same as those from phenyl ether, the mechanisms of dissociation might vary. The generation of these products in phenyl ether was greatly enhanced with the 1s → π^* transition at the C atom, but no clear enhancement of these products in 1,3-diphenoxybenzene was observed at the corresponding transition. Dissociation of phenol at a site-specific bond was observed upon excitation of a core electron of oxygen.[18] In particular, fragments corresponding to the O−H bond were much enhanced at 535.5 eV, observed only upon excitation at the oxygen K-edge, but no analogous enhancement in 1,3-diphenoxybenzene was observed. Although the branching ratios of products with m/z = 139 and 115 u (related to cleavage of the C−O bond) increase about 1% at 537 eV, corresponding to the O1,1′ → Rydberg state excitation, these products were also observed at the C K-edge; the branching ratios are much larger than those at the O K-edge.

In the dissociation of CH_3OCOCN and CH_3OCOCH_2CN after excitation at the N and O K-edges, Ibuki and co-workers investigated the effect of molecular size on the dissociation at specific sites.[73] In CH_3OCOCN, fragmentation dependent on a site or state was weak or negligible. The valence electrons are delocalized over the entire molecule, so the site of positive charge after an Auger decay would be random and an initial memory of the molecule would be lost. In contrast, CH_3OCOCH_2CN clearly showed fragmentation at a specific site and for a specific state. As in this molecule one CH_2 moiety separates the CN and CO functional groups, the valence $\pi^*_{C=O}$ and π^*_{C-N} electrons are localized; dissociation at a specific site was clearly observed in the cyanoacetate.

The destination orbitals for the transitions at the C and O K-edges of phenol, phenyl ether, and 1,3-diphenoxybenzene are highly delocalized, as shown in Figures 4b,d,f and 5b,d. Thus, an effect of size similar to that found in methyl cyanoformate and methyl cyanoacetate is not expected to occur in phenol, phenyl ether, or 1,3-diphenoxybenzene. In contrast, less site-specific dissociation was observed as the molecular size increased in going from phenol to phenyl ether to 1,3-diphenoxybenzene. A possible explanation is that the rate of intramolecular vibrational redistribution increases with increasing molecular size, as is commonly observed following UV excitation.

■ ASSOCIATED CONTENT

ⓢ Supporting Information

Spectra of phenol and phenyl ether calculated using the aug-cc-pCVTZ basis set (Figures S1 and S2); transition orbitals (Figures S3−S6); analysis of NEXAFS spectra of phenol (Figures S7−S9 and Tables S1 and S2); mass spectra of 1,3-diphenoxybenzene excited at resonant excitation energies of the oxygen K-edge (Figure S10); and possible formulas and bond cleavages of most of the major ionic products (Table S3). This material is available free of charge via the Internet at http://pubs.acs.org.

■ AUTHOR INFORMATION

Corresponding Authors
*E-mail: liu.cl@nsrrc.org.tw (C.-L.L.).
*E-mail: chewph@ccu.edu.tw (W.-P.H.).

Notes
The authors declare no competing financial interest.

■ REFERENCES

(1) Lindh, A. Zur Kenntnis des Röntgenabsorptionsspektrums von Chlor. *Z. Physik* **1921**, *6*, 303−310.

(2) Siegbahn, M. *Spektroskopie der Röntgenstrahlen*; Springer: Berlin, 1931.

(3) Vall-Ilosera, G.; Gao, B.; Kivimäki, A.; Coreno, M.; Ruiz, J. Á.; de Simone, M.; Ågren, H.; Rachlew, E. The C 1s and N 1s Near Edge X-ray Absorption Fine Structure Spectra of Five Azabenzenes in the Gas Phase. *J. Chem. Phys.* **2008**, *128*, No. 044316.

(4) Plekan, O.; Feyer, V.; Richter, R.; Coreno, M.; Vall-Ilosera, G.; Prince, K. C.; Trofimov, A. B.; Zaytseva, I. L.; Moskovskaya, T. E.; Gromov, E. V.; et al. An Experimental and Theoretical Core-Level Study of Tautomerism in Guanine. *J. Phys. Chem. A* **2009**, *113*, 9376−9385.

(5) Feyer, V.; Plekan, O.; Richter, R.; Coreno, M.; de Simone, M.; Prince, K. C.; Trofimov, A. B.; Zaytseva, I. L.; Schirmer, J. Tautomerism in Cytosine and Uracil: A Theoretical and Experimental X-ray Absorption and Resonant Auger Study. *J. Phys. Chem. A* **2010**, *114*, 10270−10276.

(6) Graf, N.; Yegen, E.; Gross, T.; Lippitz, A.; Weigel, W.; Krakert, S.; Terfort, A.; Unger, W. E. S. XPS and NEXAFS Studies of Aliphatic and Aromatic Amine Species on Functionalized Surfaces. *Surf. Sci.* **2009**, *603*, 2849−2860.

(7) Oji, H.; Mitsumoto, R.; Ito, E.; Ishii, H.; Ouchi, Y.; Seki, K.; Yokoyama, T.; Ohta, T.; Kosugi, N. Core Hole Effect in NEXAFS Spectroscopy of Polycyclic Aromatic Hydrocarbons: Benzene, Chrysene, Perylene, and Coronene. *J. Chem. Phys.* **1998**, *109*, 10409−10418.

(8) Samuel, N. T.; Lee, C.-Y.; Gamble, L. J.; Fischer, D. A.; Castner, D. G. NEXAFS Characterization of DNA Components and Molecular-Orientation of Surface-Bound DNA Oligomers. *J. Electron Spectrosc. Relat. Phenom.* **2006**, *152*, 134−142.

(9) Cooney, R. R.; Urquhart, S. G. Chemical Trends in the Near-Edge X-ray Absorption Fine Structure of Monosubstituted and Para-Bisubstituted Benzenes. *J. Phys. Chem. B* **2004**, *108*, 18185−18191.

(10) Solomon, J. L.; Madix, R. J.; Stöhr, J. Orientation and Absolute Coverage of Benzene, Aniline, and Phenol on Ag(110) Determined by NEXAFS and XPS. *Surf. Sci.* **1991**, *255*, 12−30.

(11) Eberhardt, W.; Sham, T. K.; Carr, R.; Krummacher, S.; Strongin, M.; Weng, S. L.; Wesner, D. Site-Specific Fragmentation of Small

Molecules following Soft-X-Ray Excitation. *Phys. Rev. Lett.* **1983**, *50*, 1038−1041.

(12) Eberhardt, W.; Stöhr, J.; Feldhaus, J.; Plummer, E. W.; Sette, F. Correlation between Electron Emission and Fragmentation into Ions following Soft-X-Ray Excitation of the N₂ Molecule. *Phys. Rev. Lett.* **1983**, *51*, 2370−2373.

(13) Ikenaga, E.; Isari, K.; Kudara, K.; Yasui, Y.; Sardar, S. A.; Wada, S.; Sekitani, T.; Tanaka, K.; Mase, K.; Tanaka, S. Study of Ion Desorption Induced by Carbon Core Excitation for Poly-methyl-methacrylate Thin Film Using Electron-Ion Coincidence Spectroscopy. *J. Chem. Phys.* **2001**, *114*, 2751−2759.

(14) Wada, S.-I.; Kizaki, H.; Matsumoto, Y.; Sumii, R.; Tanaka, K. Selective Chemical Bond Breaking Characteristically Induced by Resonant Core Excitation of Ester Compounds on a Surface. *J. Phys.: Condens. Matter* **2006**, *18*, S1629−S1653.

(15) Plekan, O.; Feyer, V.; Ptasińska, S.; Tsud, N.; Cháb, V.; Matolín, V.; Prince, K. C. Photoemission Study of Thymidine Adsorbed on Au(111) and Cu(110). *J. Phys. Chem. C* **2010**, *114*, 15036−15041.

(16) Baba, Y. Element-Specific and Site-Specific Ion Desorption from Adsorbed Molecules by Deep Core-Level Photoexcitation at the K-Edges. *Low Temp. Phys.* **2003**, *29*, 228−242.

(17) Baba, Y.; Yoshii, K.; Sasaki, T. A. Photon-Stimulated Ion Desorption from Condensed SiCl₄ by Resonant Excitation at the K-Edges. *Surf. Sci.* **1995**, *341*, 190−195.

(18) Lin, Y.-S.; Lu, K.-T.; Lee, Y. T.; Tseng, C.-M.; Ni, C.-K.; Liu, C.-L. Near-Edge X-ray Absorption Fine Structure Spectra and Site-Selective Dissociation of Phenol. *J. Phys. Chem. A* **2014**, *118*, 1601−1609.

(19) Guilhaus, M.; Selby, D.; Mlynski, V. Orthogonal Acceleration Time-of-Flight Mass Spectrometry. *Mass Spectrom. Rev.* **2000**, *29*, 65−107.

(20) Coles, J.; Guilhaus, M. Orthogonal Acceleration—A New Direction for Time-of-Flight Mass Spectrometry: Fast, Sensitive Mass Analysis for Continuous Ion Sources. *TrAC, Trends Anal. Chem.* **1993**, *12*, 203−213.

(21) Dawson, J. H. J.; Guilhaus, M. Orthogonal-Acceleration Time-of-Flight Mass Spectrometer. *Rapid Commun. Mass Spectrom.* **1989**, *3*, 155−159.

(22) Selby, D. S.; Mlynski, V.; Guilhaus, M. A 20 kV Orthogonal Acceleration Time-of-Flight Mass Spectrometer for Matrix-Assisted Laser Desorption/Ionization. *Int. J. Mass Spectrom.* **2001**, *210−211*, 89−100.

(23) Chung, S. C.; Chen, J.; Huang, L. R.; Wu, R. T.; Chen, C. C.; Cheng, N. F.; Chuang, J. M.; Tseng, P. C.; Huang, D. J.; Chang, C. F.; et al. Performance of an Elliptically Polarized Undulator Beamline. *Nucl. Instrum. Methods Phys. Res., Sect. A* **2001**, *467−468* (Part 1), 445−448.

(24) Sodhi, R. N. S.; Brion, C. E. Reference Energies for Inner Shell Electron Energy-Loss Spectroscopy. *J. Electron Spectrosc. Relat. Phenom.* **1984**, *34*, 363−372.

(25) Sham, T. K.; Yang, B. X.; Kirz, J.; Tse, J. S. K-Edge Near-Edge X-ray-Absorption Fine Structure of Oxygen- and Carbon-Containing Molecules in the Gas Phase. *Phys. Rev. A* **1989**, *40*, 652−669.

(26) Vall-Ilosera, G.; Huels, M. A.; Coreno, M.; Kivimäki, A.; Jakubowska, K.; Stankiewicz, M.; Rachlew, E. Photofragmentation of 2-Deoxy-D-ribose Molecules in the Gas Phase. *ChemPhysChem* **2008**, *9*, 1020−1029.

(27) Tronc, M.; King, G. C.; Read, F. H. Carbon K-Shell Excitation in Small Molecules by High-Resolution Electron Impact. *J. Phys. B: At. Mol. Phys.* **1979**, *12*, 137−157.

(28) Tronc, M.; King, G. C.; Read, F. H. Nitrogen K-Shell Excitation in N₂, NO and N₂O by High-Resolution Electron Energy-Loss Spectroscopy. *J. Phys. B: At. Mol. Phys.* **1980**, *13*, 999−1008.

(29) Wight, G. R.; Brion, C. E. K-Shell Energy Loss Spectra of 2.5 keV Electrons in CO₂ and N₂O. *J. Electron Spectrosc. Relat. Phenom.* **1974**, *3*, 191−205.

(30) Feyer, V.; Plekan, O.; Richter, R.; Coreno, M.; Prince, K. C.; Carravetta, V. Core Level Study of Alanine and Threonine. *J. Phys. Chem. A* **2008**, *112*, 7806−7815.

(31) Stöhr, J. *NEXAFS Spectroscopy*; Springer Series in Surface Sciences, Vol. *25*; Springer: Berlin, 1992.

(32) Ågren, H.; Carravetta, V.; Vahtras, O.; Pettersson, L. G. M. Direct, Atomic Orbital, Static Exchange Calculations of Photo-absorption Spectra of Large Molecules and Clusters. *Chem. Phys. Lett.* **1994**, *222*, 75−81.

(33) Ågren, H.; Carravetta, V.; Vahtras, O.; Pettersson, L. G. M. Direct SCF Direct Static-Exchange Calculations of Electronic Spectra. *Theor. Chem. Acc.* **1997**, *97*, 14−40.

(34) Stener, M.; Lisini, A.; Decleva, P. Density Functional Calculations of Excitation Energies and Oscillator Strengths for C1s → π* and O1s → π* Excitations and Ionization Potentials in Carbonyl Containing Molecules. *Chem. Phys.* **1995**, *191*, 141−154.

(35) Triguero, L.; Pettersson, L.; Ågren, H. Calculations of Near-Edge X-ray-Absorption Spectra of Gas-Phase and Chemisorbed Molecules by Means of Density-Functional and Transition-Potential Theory. *Phys. Rev. B* **1998**, *58*, 8097−8110.

(36) Rehr, J. J.; Ankudinov, A. L. Progress in the Theory and Interpretation of XANES. *Coord. Chem. Rev.* **2005**, *249*, 131−140.

(37) Nooijen, M.; Bartlett, R. J. Description of Core-Excitation Spectra by the Open-Shell Electron-Attachment Equation-of-Motion Coupled Cluster Method. *J. Chem. Phys.* **1995**, *102*, 6735−6756.

(38) Ueda, K.; Hoshino, M.; Tanaka, T.; Kitajima, M.; Tanaka, H.; De Fanis, A.; Tamenori, Y.; Ehara, M.; Oyagi, F.; Kuramoto, K.; Nakatsuji, H. Symmetry-Resolved Vibrational Spectra of Carbon K-Shell Photoelectron Satellites in Carbon Monoxides: Experiment and Theory. *Phys. Rev. Lett.* **2005**, *94*, No. 243004.

(39) Kuramoto, K.; Ehara, M.; Nakatsuji, H.; Kitajima, M.; Tanaka, H.; De Fanis, A.; Tamenori, Y.; Ueda, K. C 1s and O 1s Photoelectron Spectra of Formaldehyde with Satellites: Theory and Experiment. *J. Electron Spectrosc. Relat. Phenom.* **2005**, *142*, 253−259.

(40) Kuramoto, K.; Ehara, M.; Nakatsuji, H. Theoretical Fine Spectroscopy with Symmetry Adapted Cluster−Configuration Inter-action General-R Method: First-Row K-Shell Ionizations and Their Satellites. *J. Chem. Phys.* **2005**, *122*, No. 014304.

(41) Ehara, M.; Nakatsuji, H.; Matsumoto, M.; Hatamoto, T.; Liu, X.-J.; Lischke, T.; Prümper, G.; Tanaka, T.; Makochekanwa, C.; Hoshino, M.; et al. Symmetry-Dependent Vibrational Excitation in N 1s Photoionization of N₂: Experiment and Theory. *J. Chem. Phys.* **2006**, *124*, No. 124311.

(42) Tanaka, T.; Ueda, K.; Feifel, R.; Karlsson, L.; Tanaka, H.; Hoshino, M.; Kitajima, M.; Ehara, M.; Fukuda, R.; Tamaki, R.; et al. Symmetry and Vibrationally Resolved Absorption Spectra Near the O K Edge of N₂O: Experiment and Theory. *Chem. Phys. Lett.* **2007**, *435*, 182−187.

(43) Hunt, s. J.; Goddard, W. A., III. Excited States of H₂O Using Improved Virtual Orbitals. *Chem. Phys. Lett.* **1969**, *3*, 414−418.

(44) Besley, N. A.; Noble, A. Time-Dependent Density Functional Theory Study of the X-ray Absorption Spectroscopy of Acetylene, Ethylene, and Benzene on Si(100). *J. Phys. Chem. C* **2007**, *111*, 3333−3340.

(45) Besley, N. A.; Asmuruf, F. A. Time-Dependent Density Functional Theory Calculations of the Spectroscopy of Core Electrons. *Phys. Chem. Chem. Phys.* **2010**, *12*, 12024−12039.

(46) Stener, M.; Fronzoni, G.; de Simone, M. Time Dependent Density Functional Theory of Core Electrons Excitations. *Chem. Phys. Lett.* **2003**, *373*, 115−123.

(47) Bunău, O.; Joly, Y. Time-Dependent Density Functional Theory Applied to X-ray Absorption Spectroscopy. *Phys. Rev. B* **2012**, *85*, No. 155121.

(48) Hirata, S.; Head-Gordon, M. Time-Dependent Density Functional Theory within the Tamm−Dancoff Approximation. *Chem. Phys. Lett.* **1999**, *314*, 291−299.

(49) Fronzoni, G.; Stener, M.; Reduce, A.; Decleva, P. Time-Dependent Density Functional Theory Calculations of Ligand K Edge and Metal L Edge X-ray Absorption of a Series of Oxomolybdenum Complexes. *J. Phys. Chem. A* **2004**, *108*, 8467−8477.

(50) Fronzoni, G.; De Francesco, R.; Stener, M. Time Dependent Density Functional Theory of X-ray Absorption Spectroscopy of Alkaline-Earth Oxides. *J. Phys. Chem. B* **2005**, *109*, 10332−10340.

(51) Fronzoni, G.; De Francesco, R.; Stener, M.; Causà, M. X-ray Absorption Spectroscopy of Titanium Oxide by Time Dependent Density Functional Calculations. *J. Phys. Chem. B* **2006**, *110*, 9899−9907.

(52) van Leeuwen, R.; Baerends, E. J. Exchange−Correlation Potential with Correct Asymptotic Behavior. *Phys. Rev. A* **1994**, *49*, 2421−2431.

(53) Imamura, Y.; Nakai, H. Time-Dependent Density Functional Theory (TDDFT) Calculations for Core-Excited States: Assessment of an Exchange Functional Combining the Becke88 and Van Leeuwen−Baerends-Type Functionals. *Chem. Phys. Lett.* **2006**, *419*, 297−303.

(54) Feller, D. The Role of Databases in Support of Computational Chemistry Calculations. *J. Comput. Chem.* **1996**, *17*, 1571−1586.

(55) Schuchardt, K. L.; Didier, B. T.; Elsethagen, T.; Sun, L.; Gurumoorthi, V.; Chase, J.; Li, J.; Windus, T. L. Basis Set Exchange: A Community Database for Computational Sciences. *J. Chem. Inf. Model.* **2007**, *47*, 1045−1052.

(56) Dunning, T. H. Gaussian Basis Sets for Use in Correlated Molecular Calculations. I. The Atoms Boron through Neon and Hydrogen. *J. Chem. Phys.* **1989**, *90*, 1007−1023.

(57) Woon, D. E.; Dunning, T. H. Gaussian Basis Sets for Use in Correlated Molecular Calculations. V. Core-Valence Basis Sets for Boron through Neon. *J. Chem. Phys.* **1995**, *103*, 4572−4585.

(58) Frisch, M. J.; Trucks, G. W.; Schlegel, H. B.; Scuseria, G. E.; Robb, M. A.; Cheeseman, J. R.; Scalmani, G.; Barone, V.; Mennucci, B.; Petersson, G. A.; et al. *Gaussian 09*, revision D; Gaussian, Inc.: Wallingford, CT, 2009.

(59) Shao, Y.; Molnar, L. F.; Jung, Y.; Kussmann, J.; Ochsenfeld, C.; Brown, S. T.; Gilbert, A. T. B.; Slipchenko, L. V.; Levchenko, S. V.; O'Neill, D. P.; et al. Advances in Methods and Algorithms in a Modern Quantum Chemistry Program Package. *Phys. Chem. Chem. Phys.* **2006**, *8*, 3172−3191.

(60) Zhao, Y.; Truhlar, D. The M06 Suite of Density Functionals for Main Group Thermochemistry, Thermochemical Kinetics, Non-covalent Interactions, Excited States, and Transition Elements: Two New Functionals and Systematic Testing of Four M06-Class Functionals and 12 Other Functionals. *Theor. Chem. Acc.* **2008**, *120*, 215−241.

(61) Plashkevych, O.; Yang, L.; Vahtras, O.; Ågren, H.; Petterson, L. G. Substituted Benzenes as Building Blocks in Near-Edge X-ray Absorption Spectra. *Chem. Phys.* **1997**, *222*, 125−137.

(62) Tsai, S.-T.; Lin, C.-K.; Lee, Y. T.; Ni, C.-K. Dissociation Rate of Hot Benzene. *J. Chem. Phys.* **2000**, *113*, 67−70.

(63) (a) *NIST Chemistry WebBook*; Linstrom, P. J., Mallard, W. G., Eds.; NIST Standard Reference Database Number 69; http://webbook.nist.gov. (b) Mass Spectrometry Data Center. http://chemdata.nist.gov.

(64) Tseng, C.-M.; Lee, Y. T.; Lin, M.-F.; Ni, C.-K.; Liu, S.-Y.; Lee, Y.-P.; Xu, Z. F.; Lin, M. C. Photodissociation Dynamics of Phenol. *J. Phys. Chem. A* **2007**, *111*, 9463−9470.

(65) Le, H. T.; Flammang, R.; Gerbaux, P.; Bouchoux, G.; Nguyen, M. T. Ionized Phenol and Its Isomers in the Gas Phase. *J. Phys. Chem. A* **2001**, *105*, 11582−11592.

(66) Lin, C.-K.; Huang, C.-L.; Jiang, J.-C.; Chang, A. H. H.; Lee, Y. T.; Lin, S. H.; Ni, C.-K. Photoisomerization and Photodissociation of Toluene in Molecular Beam. *J. Am. Chem. Soc.* **2002**, *124*, 4068−4075.

(67) Sakai, M.; Okada, K.; Ohne, K.; Tabayashi, K. Specific Fragmentation of the K-Shell Excited/Ionized Pyridine Derivatives Studied by Electron Impact: 2-, 3- and 4-Methylpyridine. *J. Mass Spectrom.* **2010**, *45*, 306−312.

(68) Kawasaki, R.; Yamanaka, T.; Tabayashi, K.; Hiroaki, Y. Site- and State-Selective Dissociation of Core-Excited Organic Molecules: Deuterium-Labeled Methyl Acetate. *J. Nucl. Sci. Technol., Suppl. 6* **2008**, 19−23.

(69) Stolte, W. C.; Ohrwall, G.; Sant'Anna, M. M.; Lopez, I. D.; Dang, L. T. N.; Piancastelli, M. N.; Lindle, D. W. 100% Site-Selective Fragmentation in Core-Hole-Photoexcited Methanol by Anion-Yield Spectroscopy. *J. Phys. B: At., Mol. Opt. Phys.* **2002**, *35*, L253−L259.

(70) Piancastelli, M. N.; Stolte, W. C.; Guillemin, R.; Wolska, A.; Yu, S. W.; Sant'Anna, M. M.; Lindle, D. W. Anion and Cation-Yield Spectroscopy of Core-Excited SF_6. *J. Chem. Phys.* **2005**, *122*, No. 094312.

(71) Stolte, W. C.; Hansen, D. L.; Piancastelli, M. N.; Dominguez Lopez, I.; Rizvi, A.; Hemmers, O.; Wang, H.; Schlachter, A. S.; Lubell, M. S.; Lindle, D. W. Anionic Photofragmentation of CO: A Selective Probe of Core-Level Resonances. *Phys. Rev. Lett.* **2001**, *86*, 4504−4507.

(72) Stolte, W. C.; Dumitriu, I.; Yu, S. W.; Ohrwall, G.; Piancastelli, M. N.; Lindle, D. W. Fragmentation Properties of Three-Membered Heterocyclic Molecules by Partial Ion Yield Spectroscopy: C_2H_4O and C_2H_4S. *J. Chem. Phys.* **2009**, *131*, No. 174306.

(73) Ibuki, T.; Okada, K.; Saito, K.; Gejo, T. Molecular Size Effect on the Site-Specific Fragmentation of N and O K Shell Excited CH_3OCOCN and CH_3OCOCH_2CN Molecules. *J. Electron Spectrosc. Relat. Phenom.* **2000**, *107*, 39−47.